Proper orthogonal decomposition analysis of variable temperature field during gas tungsten arc welding

Nicolas Blanc, T. Boutin, Issam Bendaoud, Fabien Soulié, Cyril Bordreuil

Proper Orthogonal Decomposition analysis of Variable Temperature Field During Gas Tungsten Arc Welding

N.Blanc,[1] T.Boutin,[1] I.Bendaoud,[1] F.Soulié,[1] and C.Bordreuil[1, a)]
LMGC, Univ. Montpellier, CNRS Montpellier, France

Fluid flow motion controls energy transfer in the weld pool and drives solidification process. Experimental investigation of fluid flow during welding is made particularly difficult by unsteady movements in the molten pool. In this paper, proper orthogonal decomposition (POD) based on images during gas tungsten arc welding (GTAW) on thin plates is used to investigate coherent structures revealed by thermal field in the molten pool. The POD method is based on fluctuating gray levels related to surface temperature. Based on this decomposition, two dimensional spatial modes and temporal coefficients are calculated allowing the identification of regions where temperatures are correlated. To explore the potential of POD method, weld beads were performed on 316L stainless steel plate at three welding speeds (2.3, 3.3 and 4.3 $mm.s^{-1}$) and constant current (80A). These three conditions lead to different sizes of fully penetrated weld pools and different temperature distributions. Spatial modes and temporal coefficients provide information on temperature fluctuations along the free surface. Based on POD first modes, thermal field is reconstructed along the free surface to understand the heat transfer. Combining these results with side-view observations of the arc allows us to derive three dimensional flow patterns within the weld pool.

Keywords: Gas Tungsten Arc Welding, Fluid flow, POD

I. INTRODUCTION

Arc welding is widely used in aerospace, automotive and power generation industries, and is used to join two metallic parts with a localized energy density. A heat input initiates complex physical and chemical processes, namely metal melting and solidification or fluid flow and vaporization. The final geometry of the weld and its metallurgical structure are controlled by fluid flow and heat transfer in the molten pool. Understanding the distribution of temperatures in the weld pool is then important for assessing the quality of welded joints.

Fluid flow is driven by different forces acting in the liquid metal or at the weld pool surface and is highly coupled to thermal field. Buoyancy forces, Lorentz forces, shear stresses induced by the arc plasma, arc pressure and Marangoni stresses drive complex fluid flow inside the weld pool.

To understand fluid dynamic phenomena and the associated heat transfer in the weld pool during gas tungsten arc welding (GTAW), Tanaka *et al*[1] developed a model that couples plasma physics and laminar incompressible fluid flow in the base material. This model was used to investigate the influence of the Marangoni effect on fluid flows and on weld geometries. Traida[2] developed a similar model but this time taking into account the deformation of the free surface to investigate flow pattern in horizontal and vertical positions. With numerical simulations, Chakraborty[3] analyzed the effect of turbulent transport during the arc welding process and demonstrated its significant influence on the geometries of the weld pool and temperature distribution in the liquid. More recently, Kidess[4] investigated the stability inside a molten pool during laser spot welding. They used large eddy simulation and direct numerical simulation to study the influence of the Marangoni number on the flow regimes (laminar, turbulent or chaotic) and the geometry of the molten pool.

Although numerical simulations are powerful tools with which to understand the relationship between physics and process parameters, they can not always take into account uncertainties and possible fluctuations in geometry. For this reason, experimental methods have been developed to study fluid flow and heat transfer. Kraus investigated weld pool flow motion by measuring weld pool temperature[5] on a 304L stainless steel plate. This latter work was then completed by a numerical study[6]. Kraus revealed the presence of several fluid flow cells similar to Bénard cells. More recently, different authors developed methods to measure and investigate fluid flow in GTAW based on direct observations. Henrikson[7] observed weld pool surface flow with a high speed camera during GTAW of stainless steel by tracking seed particles introduced as markers. With his experimental conditions, he measured a velocity inside the weld pool around $0.13\,m.s^{-1}$. Zhao[8,9] used the same experimental configuration to investigate surface fluid flow based on particle image velocimetry (PIV). For 80 A and a welding velocity of $4\,mm.s^{-1}$ with a 500 Hz frame rate, he measured a fluid velocity around $0.1\,m.s^{-1}$ and demonstrated that the fluid flow was unsteady with rotational inward and outward motions. He decomposed the surface velocity field in different modes and measured the clockwise and counter-clockwise vortices which can be due to an instability phenomena. With these maximum velocities, the Reynolds number ranged between 600 and 3000. These values outline the relationship between of kinetic versus viscosity effects. More recently, X-ray synchrotron experiments[10] were used to investigate internal flow during melt-pool-based metal manufacturing. Based on images, the geometric evolution of the melt pool was plotted over time. It was possible to measure fluid flow dynamics by using tungsten and tantalum particles as tracers that moved according to the flow. Particles paths showed the presence of several flow patterns in the melt pool.

a)Electronic mail: cyril.bordreuil@umontpellier.fr

For these experimental conditions, velocities up to $0.5\,m.s^{-1}$ were measured in the bulk. These experiments are very impressive from a scientific point of view but their results are difficult to interpret in the context of real welding conditions.

In real operating conditions, the weld pool often shows turbulence in the bulk which is difficult to investigate[8]. In the field of turbulence, Proper Orthogonal Decomposition (POD)[11–13] is often used to investigate the apparent random vector field representing turbulent fluid flow by decomposing the value vector in spatial modes, which can provide information about the organisation of the flow. The POD method can also be applied to scalar fields like temperature. The originality of this paper lies in the fact that we apply POD to experimental observations similar to Zhao[8] but without any external particles that can modify the fluid flow. More particularly, the purpose of this study is to use POD to investigate the variable temperature field within the weld pool which provides some information on the flow pattern.

The following section of this paper describes the experimental setup. Section III describes the POD method applied to obtained images. Section IV shows the experimental and POD results. The last section discusses fluid flow pattern derived from the spatial modes obtained by POD.

II. EXPERIMENTAL METHOD

A. Experimental set-up

A schematic diagram of the experiment is presented in figure 1. The set-up consists of a GTAW torch, a plate and a camera. A 2.4 mm diameter tungsten electrode with 2 % lanthanum, with a 30 degrees grinding angle, is positioned at 3 mm away from the sample during welding. A 28.6 mm diameter nozzle releases pure argon at 15 L/min to shield the liquid metal on the arc side. The 316L stainless steel plate is clamped on a guided motorized stand to produce a 100mm bead on plate with a fully penetrated weld pool. An independent flow of argon fills a chamber underneath the plate (shown in purple in figure 1) in order to purge oxygen and protect the weld pool from oxidation. The arc is initiated by lift-arc procedure at the beginning of the experiment and the table begins to move 0.4 s after arc initiation. We chose to perform three different experimental tests, with three different welding speeds w_x of 2.3, 3.3 and 4.3 mm/s. The welding current was kept at 80 A. These conditions create a full penetrated weld pool.

The energy delivered by the welding generator is monitored by measuring the current I and the arc voltage U. The average of these two measurements are given in table I. Arc voltage and current were almost constant, indicating that the electrical power input is similar for the three conditions. Therefore, tests can be compared on the basis of welding speeds or linear energy.

On the bottom side of the plate, a glass allowed to observe the weld pool with a camera (800x600 pixels, Mako, Allied Vision Technologies) at 300 frames per second (figure 1) without any spectral filter. Each pixel is encoded in 8 bits. A 808 nm laser light with a power of 15 W is positioned to illuminate the weld pool. The laser beam is not collimated and is tilted at 45° from the vertical axis. The laser beam is used mainly to obtain a better contrast between the molten metal and its solid surroundings which have different reflection factors. This low power input compared to 700W of the electric arc is assumed to not modify the heat transfer. Other cameras were used to observe the weld pool on the side of the arc. Solidification phenomena were also measured but investigation of these is beyond the scope of the present paper (see[14]).

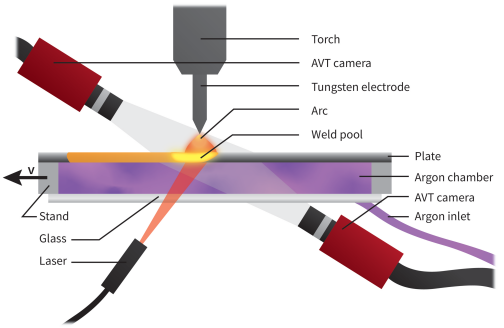

FIG. 1. Diagram of the experimental set-up.

TABLE I. Average current, arc voltage and linear energy for the three different welding speed.

Welding speed (mm/s)	I (A)	U (V)	E_l (J/mm)
2.3	81.7	8.58	305
3.3	81.3	8.76	216
4.3	81.5	8.67	164

B. Material

The material is 316L stainless steel. The plate dimensions are 150 (L) x 70 (W) x1.5 (T) mm^3. It is difficult to measure thermo-physical properties at liquid state. Specific properties have been taken from the literature, see table II. It is assumed that the surface tension gradient constant is negative meaning that for positive temperature gradient, the Marangoni effect causes the liquid to flow away from high-temperature regions to low-temperatures regions[16].

TABLE II. Thermo Physical material properties of 316L stainless steel at liquid state

Symbol	Property	Value	Reference
ρ	mass density	6250 $kg.m^{-3}$	1
$\frac{d\sigma}{dT}$	Surface tension gradient	$-4.58.10^{-4} N.m^{-1}.K-1$	1
μ	dynamic viscosity	0.006 $kg.m^{-1}.s^{-1}$	9
c	thermal capacity	720 $J.Kg^{-1}.K^{-1}$	1
k	thermal conductivity	20 $W.m^{-1}.K^{-1}$	1
T_s	Solidus	1658 K	15
Pr	Prandtl Number $(\mu c_p/k)$	0.22	

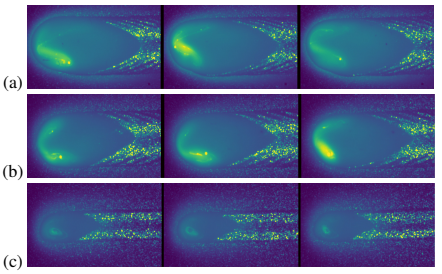

FIG. 2. Raw images of the weld pool for different welding speeds. (a) 2.3mm/s welding speed (multimedia view)- (b) 3.3mm/s (multimedia view)- (c) 4.3mm/s (multimedia view)

C. Raw images

Figure 2 presents raw images obtained for the different welding speeds at different times during a test. The exposure time is kept at 20 μs for the three welding speeds in order to maintain an unsaturated gray level. Due to this small exposure time, the images remains sharp and in focus. If gray levels are plotted along a line in an image, the values are not smooth. The relative error of the measurement can be estimated at 3 to 5 per cent of the value.

Thanks to the laser lighting, the solid and liquid parts on the bottom side are easily observed due to the difference of texture. The size and the shape of the molten pool can also be measured. For the first welding speed (Fig 2(a)), the position and value of the maximum gray level evolve with time, showing that there is significant transfer inside the weld pool. The camera detects mainly the spectral radiance of the liquid surface. It is assumed that the free surface does not evolve significantly during the test meaning that the angle between the surface and the camera can be considered constant. It can also be assumed that changes in gray level inside the weld pool are due to modification of gray level (spectral radiance) in accordance to Planck's law:

$$N_g = k\varepsilon \int_\lambda \frac{C_1 \lambda^{-5}}{exp(\frac{C_2}{\lambda T}) - 1} d\lambda \quad (1)$$

where N_g is the gray level, k is a calibration coefficient, ε the emissivity of the liquid and T the surface temperature in K. The constant coefficients C_1 and C_2 are the two Planck constants. For liquid stainless steel, temperature can be between 1500K and 3000K. In this range, the relationship between the surface temperature and the gray level resembles an increasing downward parabola. The function is monotonic and temperature is therefore directly proportional for one gray level.

For the two first conditions (2.3mm/s figure 2(a) (multimedia view) and 3.3 mm/s figure 2(b) (multimedia view)), videos show particles (bubbles in fact) and regions with high gray levels moving from one side of the weld pool to the other. This demonstrates that there are large oscillations in the weld pool for these welding parameters. Small vortices can also be observed inside the main fluid flow. No oscillations are visible with a welding speed of 4.3mm/s(figure 2 (c) (multimedia view)). For this condition, there are two vortices: one large vortex at the bottom and one small at the top in figure 2(c) (multimedia view). These experiments were repeated several times and the pulsatile motion was observed for the two first welding speeds each time. The two vortices for 4.3mm/s were commonly encountered during weld bead on plate.

As shown in figure 1, the camera is tilted, and so a calibration procedure is applied to correct the image in the plane of the plate[17].

III. PROPER ORTHOGONAL DECOMPOSITION BASED ON GRAY LEVEL

A. Principles

Proper orthogonal decomposition is used to study turbulence and cyclic variation of flow and is considered as an efficient tool with which to identify coherent structures in turbulent flows[18]. Generally, POD is used to separate fluctuations in unsteady flows in simulations or in experiments. In fluid flow experiments, it is generally based on PIV (see section I) which gives a velocity field as an input for POD. POD can be used with a vector field but it can also be used with any scalar.

In a welding pool, there is a strong coupling between energy balance and momentum balance. Marangoni number is around 9.4×10^4 (see[9]). This number indicates that the flow is mainly driven by the dependence of the surface tension on the temperature, as opposed to viscous effects. Moreover, Péclet Number can be estimated to be around 200. This indicates a strong effect of advection compared to diffusion in the liquid metal. It is therefore interesting to analyze surface temperatures of weld pool with POD method in order to investigate the flow patterns.

The POD technique decomposes the gray level scalar field into a sum of weighted linear modes $\phi_m(x,y)$. These spatial modes are generated from a sample of snapshots. The sample

corresponds to a series of m images acquired at a given frequency f_s. A region of interest (see section III B) is defined in one image and is kept constant for every snapshots. Here, it can be considered as a rectangular domain with M rows and N columns. At each time-point, the gray level matrix is flattened in a vector of gray level. This vector is denoted $N_g(x_i, y_j, t_l)$ for each point (x_i, y_j) in the region of interest at time t_l. The snapshots corresponding to gray level values in the region of interest are stored in a matrix format in which a row corresponds to values at time t_l:

$$\mathbf{N} = \begin{bmatrix} N_g(x_1, y_1, t_1) & \dots & N_g(x_M, y_N, t_1) \\ \vdots & \dots & \vdots \\ N_g(x_1, y_1, t_m) & \dots & N_g(x_M, y_N, t_m) \end{bmatrix} \quad (2)$$

Because POD is efficient in tackling fluctuations, the mean value at each point over time must be computed:

$$\bar{\mathbf{N}}(x_i, y_j) = mean_{t_l}(N(x_i, y_j, t_l)) \quad (3)$$

Then, the matrix $\mathbf{U}$ is defined as:

$$\mathbf{U} = \mathbf{N} - \bar{\mathbf{N}} \quad (4)$$

This operation corresponds to subtracting the mean value at each point in the region of interest. In the present work, the snapshot POD introduced by Sirovich[19] is used because the problem has less snapshots than grid points. The correlation matrix is then built as :

$$\mathbf{C}_s = \frac{1}{m-1}\mathbf{U}\mathbf{U}^T \quad (5)$$

This matrix has $m \times m$ rows and columns. Eigen modes $\mathbf{A}_s$ and eigenvalues λ_s of matrix $\mathbf{C}_s$ are computed. Eigen modes $\mathbf{A}_s$ are temporal modes. To obtain spatial modes, gray level datas are projected onto temporal modes:

$$\phi_s = \mathbf{U}^T \mathbf{A}_s \quad (6)$$

Each column of matrix ϕ_s contains spatial modes ordered from the largest to the lowest eigenvalues. These modes optimally capture the energy of the unsteady flow field and the eigenvalues represent the amount of energy held by each mode. At this stage, the vector of size $M \times N$ (corresponding to the number of grid points) for a mode ϕ_i is normalized by its maximum value. This value is multiplied to the corresponding temporal coefficient $(\mathbf{A}_s)_i$. The vector ϕ_i is resized in a matrix of M rows and N columns to visualize the spatial distribution.

Equation 6 can be expressed as the sum of the contribution of each mode:

$$\tilde{\mathbf{U}} = \sum_{k=1}^{n} a_k(t)\phi_k \quad (7)$$

where $a_k(t)$ are temporal coefficients associated to spatial modes ϕ_k. Equation 7 means that the original gray level fluctuations $\tilde{\mathbf{U}}$ are decomposed into a sum of contributions from n first proper orthogonal modes. This equation is often used to reconstruct, smooth or reduce the field under study.

The number of consecutive snapshots m may influence the result in the case of very transient flow. However in this study, oscillations are well established which means that once they appear, they remain until the end of the test. If m is chosen such that two oscillations are captured throughout all snapshots, the results will be independent. Here, we use $m = 600$.

B. Region of interest

POD is successfully applied to rectangular domain (M rows and N columns). The weld pool has a more complex geometry (see figure 3). The method used here to adapt POD to non rectangular domain is as follows. Fluid flow is limited to the weld pool in the center of the images. The molten pool geometry evolves only slightly over a timescale of few seconds. Depending on welding parameters, the weld pool can have different shapes and sizes. The molten pool can be delimited by a polygon in the frame of the image. Therefore, it is straightforward to find point (x_i, y_j) inside the polygon in every snapshot. All the points are then arranged in the snapshot vector $\mathbf{N}$ (Eq. 2). This procedure has to be inverted in order to retrieve the spatial modes in the frame of the image. An example of the region of interest is shown in figure 3.

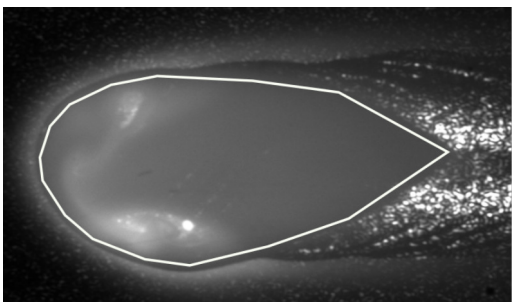

FIG. 3. Region of interest for a weld speed of 2.3mm/s after the calibration procedure; the image shows the view from below the plate.

Edge detection is possible and was done[14] based on these images; this allows us to study the change in the geometry of the weld pool throughout the welding process. In this work, the region of interest is selected manually. A polygon is defined in a reference image in order to not integrate fluctuations of the weld pool border due to possible high flow pattern. The gray level field inside the polygon is then reordered in a vector to be included in the snapshot matrix $\mathbf{U}$. The algorithm used to detect pixels inside the polygon gathers pixels by adjacent pixels in a row of the image in the vector $\mathbf{U}$.

IV. RESULTS

Before presenting our results, we summarized the procedure we use to apply the POD method to weld pool images. The first step is the definition of the region of interest. The second step consists in extracting the average gray level of snapshots for points inside the region of interest. In a third step, the POD method is applied to fluctuations. In the following section, we discuss and compare the results for these different stages.

For every experimental test, we extract 600 images to be used as snapshots. The images are taken when the weld pool geometry evolves only slightly. This corresponds to times between 10 to 20 seconds after arc initiation depending on the experimental test. Different intervals were used in the POD procedure but as outlined earlier, the results were almost the same.

A. Region of interest

The bottom surface of the molten pool can be delimited by a polygon. Due to the small thickness of the plate, the volume can be calculated starting from this surface. Then, the size of the bounding box of the polygon indicates the volume of the liquid part and the characteristic lengths inside the liquid. The results are shown in table III.

TABLE III. Geometrical characteristics of the region of interest.

Welding speed (mm/s)	Length (mm)	Width (mm)
2.3	15.44	7.23
3.3	11.96	5.06
4.3	6.86	2.46

A comparison of the dimensions of the liquid part indicates a wider and longer weld pool for the two lowest welding speeds. For the third condition (4.3mm/s), the weld pool is smaller but more elongated. For all experimental conditions, the ratios of characteristics lengths (length over width) are between 2 and 3. The lower surface of the melt-pool tends to become a teardrop shaped with increasing welding speed.

B. Mean gray level

The mean gray level is computed inside the region of interest for every point. Saturated values are not taken into account in the computation of the average value (equation 3). The mean gray levels for every point in the region of interest is plotted in figure 4 for the three tests.

If a line is plotted inside the melt-pool, the solidus can be approximated to a gray level of 60. Based on the results shown in figure 4, the maximum gray level and the mean gray level inside the molten pool can be computed (table IV) for each experimental condition.

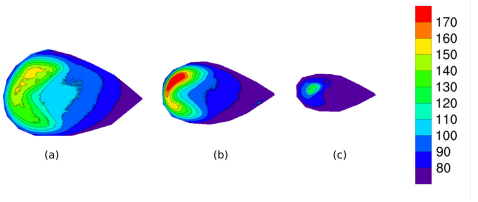

FIG. 4. Mean gray level for the three conditions - (a) 2.3mm/s, (b) 3.3mm/s, (c) 4.3 mm/s at the bottom side of the weld pool.

TABLE IV. Maximum and Mean gray level in the region of interest for the three different welding velocities.

Welding speed (mm/s)	Maximum gray level	Mean gray level
2.3	160	104
3.3	190	98
4.3	130	80

The fields of figure 4 are directly related to the distribution of the temperature at the surface opposite the arc. The distribution of the mean gray level is similar for the first two welding speeds. A zone with a higher temperature is located near the fusion front. This zone is crescent shaped. It can be related to the two vortices on each side of the centerline. The gray level field seems to be asymmetric, with a higher gray level on the left side of the weld bead (the side toward the top in the images of figure 4). The shape of the maximum gray level is wider for a welding speed of 2.3mm/s and the peak value is lower than for 3.3mm/s welding condition. This implies a smaller gradient inside the weld pool for the lower welding speed. At 4.3mm/s, the maximum value is more centered in the weld pool. This may be due to the fact that the flow is more directed from the upper side of the weld pool- where the arc illuminates the liquid metal- to the bottom side.

Flow velocity is driven by Marangoni stresses and the flow goes from the hot regions to the cold ones (see section (V) Discussions). the fluid flow due to the mean temperature in figure 4 goes away from the center of the weld pool to the fusion front.

C. Spatial modes

After matrix $\mathbf{U}$ is computed (equation 4), the procedure described by equation 5 is applied (eigenvalues and eigenmodes computation and spatial modes projection (equation 6)). Figure 5 presents the spatial distribution of mode 1 which corresponds to the highest eigenvalue for the three welding speeds. For the 2.3mm/s and 3.3mm/s speeds, two asymmetrical regions, each with one peak value, are visible along the line delimiting the middle of the weld pool. The maximum positive values on one side of this line are almost matched by the negative values on the other, indicating asymmetry in space for the

evolution of the gray level. Videos indicate a flow pattern going from the region with maximum temperature to the region with minimum temperature. The important characteristic of the mode for gray level is that when the red region becomes hotter, the blue region becomes colder and vice-versa depending on the value of the temporal coefficient.

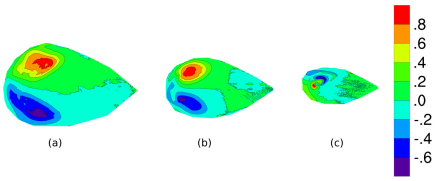

FIG. 5. Spatial distribution of mode 1 - (a) 2.3mm/s, (b) 3.3mm/s, (c) 4.3 mm/s

A precise comparison of the mode is not possible with this figure 5 because fields are normalized. It is nevertheless interesting to notice the similar structures (spatial mode distribution) for the first two experimental conditions. The temporal coefficients corresponding to this mode are plotted in figure 6. For each time, the value of the coefficient a_1 can be multiplied with the spatial mode in figure 5 to give the fluctuations of gray level corresponding to this mode. In figure 6, a comparison between the coefficients a_1 for the three welding speeds reveals an oscillatory behaviour for the two first welding conditions whereas no oscillation is observed on the third one (4.3mm/s).

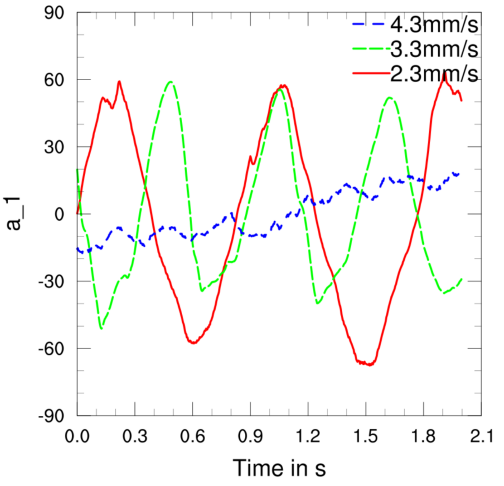

FIG. 6. Temporal coefficients for mode 1

In figure 6, the temporal coefficients resemble a sinusoidal type function with noise. Their evolution can be considered periodic. Based on the time evolution, the amplitude and the frequency of the oscillations can be computed for the fluctuations corresponding to the first spatial mode. The amplitude seems higher for 2.3mm/s than for 3.3mm/s for the chosen 600-snapshots interval. The frequency seems to be higher for the higher welding speed of 3.3mm/s. To identify the amplitude and the frequency, a least square procedure is used to fit the temporal coefficients with a sine function of the form $(A_i sin(2\pi f_i t + \phi))$. The results for amplitude (A_i) and frequencies (f_i) are given in table V.

Figure 7 shows the spatial distribution for the second mode. This mode maintains the asymmetry observed for mode 1. Two peaks are now visible on each side of the center line. For the welding speed of 3.3mm/s, the peak toward the back of the molten pool is less pronounced that the one toward the front. Once again, red regions become hotter at the same time when blue regions become colder. The evolution of the temporal coefficients corresponding to this mode is shown in figure 8. The amplitude and the frequency are computed with the same method as the previous mode and the results are also given in table V. Figure 8 shows that the amplitude for the second mode is higher for higher welding speed of 3.3mm/s than 2.3mm/s.

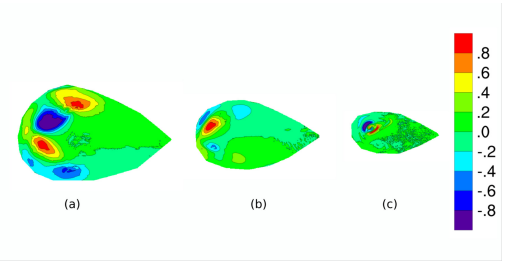

FIG. 7. Spatial distribution of mode 2 - (a) 2.3mm/s, (b) 3.3mm/s, (c) 4.3 mm/s

TABLE V. Amplitude A_i and frequency f_i for temporal coefficients $a_i(t)$ measured for the welding conditions for the first two modes. NA means no oscillation was found.

w_s (mm/s)	A_1	f_1	A_2	f_2
2.3	55	1.13	34	1.14
3.3	50	1.73	46	1.72
4.3	NA	NA	NA	NA

Table V compares the amplitude and the frequencies identified on the temporal coefficients in figures 6 and 8. It appears that the frequencies for the modes 1 and 2 are almost the same for each welding condition. For the welding speed of 3.3mm/s, the amplitudes of the first two modes are almost identical whereas for 2.3mm/s the amplitudes seems to decrease with increasing mode number. At this stage, it is inter-

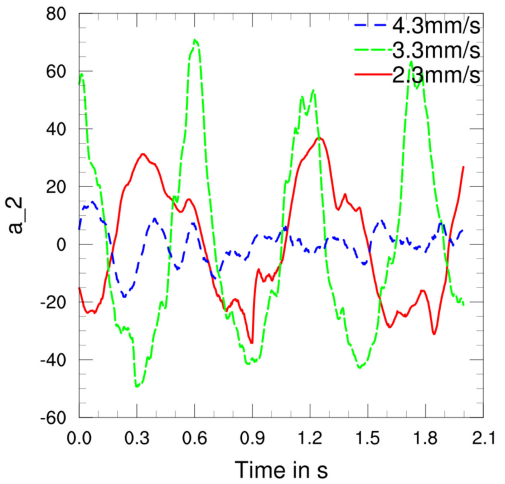

FIG. 8. Temporal coefficients for mode 2

esting to notice that results of spatial modes in figures 5 and 7 show the longest wavelength for the first mode and that the number of peaks on each side of the molten pool is proportional to the mode number.

V. DISCUSSIONS

For the first two welding speeds, the videos show a flow pattern that oscillates from one side of the bottom surface of the weld pool to the other side. A correlation can be seen between the evolution of the temporal coefficients of the first two spatial modes.

In this section, fluctuations in fluid velocities are discussed based on the proper orthogonal decomposition results of gray levels. Energy transfer is then discussed based on reconstruction of the gray level. Finally, we discuss complex flow pattern in the weld pool based on POD.

A. Fluid velocities

Here, we develop our methodology to measure fluid velocity based on the first mode of the POD. The temporal coefficients (Figures 6 and 8) oscillate between positive and negative values of equal proportion. This means there is a gradient of temperature from one side of the weld pool to the other side leading to transfer of the heat from one side to the other due high Marangoni stresses. The flow pattern that we find indicates possible fluid flow from the blue region to the red region in figure 5. In this context, it appears that the half period of the temporal coefficient could represent the time for the fluid to go from a blue patch to a red patch. The videos reveal (figure 2 (a) (multimedia view)) that the flow path from one region to the other can be approximated as a circle arc. The diameter of this circle can be considered as the width of the weld pool. The fluid velocity can be estimated based on this assumption. First, the mean fluid velocities can be computed considering that the length along the the circle arc is travelled during a half period (see table V). The mean velocity is then computed with $\bar{v} = \pi L f_1$ where L is the width of the weld pool and f_1 is the frequency of first mode given in table V.

TABLE VI. Mean velocity along a circle arc based on width and frequency ($v = \pi L f$) for mode 1 and max velocity assuming a parabolic profile $v = at^2 + bt + c$.

w_s (mm/s)	Mean velocity mm/s	Max velocity mm/s
2.3	25	39
3.3	27	41

At the beginning and at the end of flow motion between two regions, the fluid can be considered at rest. If a parabolic ($v = at^2 + bt + c$) profile of velocity is considered along the circle, it is straightforward to find coefficients by considering null velocity at the beginning and end of a half period and to integrate the velocity along the trajectory in order to find the length of the path equal to $\pi L/2$. The maximum velocity is determine by finding the time corresponding to a null derivative of the velocity. The results for these two velocities are given in table VI.

Peclet and Reynolds Number can be computed. The Peclet is around 15 at mean velocity value and around 25 at maximum velocity indicating that advection is the major driver of the fluid motion and not diffusion. With a low Prandtl number, this means that the temperature can be considered to be advected by the flow. This also confirms the assumption proposed in section I that the investigation of temperature or gray level can reveal the fluid flow. The Reynolds is around 75 at mean velocity and 110 at the maximum velocity, under the 2000 classical limit value for turbulence. These velocities are only a part of the real velocity because the mean temperature distribution induced also a velocity field. Adimensional numbers computed with the velocities of the table VI are lower bound values. The velocity field near the bottom free surface can be decomposed with two components: one tangent to the surface and one normal to it. The calculated velocities represent those of the component tangent to the free surface.

The Marangoni number can be computed as $-\frac{d\sigma}{dT} L_c \Delta T / \nu / \alpha$. It compares the rate of transport due to Marangoni flows to transport due to diffusion. Here, ΔT is the difference between the peak temperature in the molten pool and that of the Solidus, L_c is the width of the weld pool. Rivas[20] related the Marangoni number to maximum fluid velocities. For the two welding speeds that lead to oscillations in the temporal coefficient, the Marangoni numbers computed with gray level in Table IV are very similar. This explains why the velocities for the two welding conditions with oscillations are similar. Physically, it can be explained by

the fact that the temperature gradient is higher for 3.3mm/s, which tends to accelerate the fluid, but the characteristic length is smaller than for the 2.3mm/s condition, and so a shorter distance is available to accelerate the fluid particles.

B. Unsteady thermal field

The POD is performed with images of the bottom surface of the molten pool. Temperature is advected by the velocity field. It is difficult to understand the distribution of heat with images alone due to the presence of multiple flow cells.

Eigenvalues of each modes are given in figure 9 for the first welding condition (2.3mm/s).

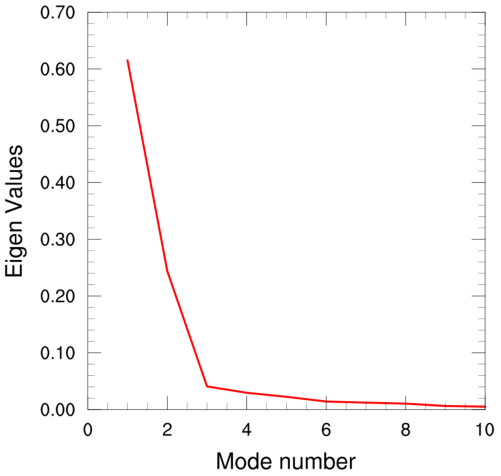

FIG. 9. Eigenvalues in function of the mode number for 2.3mm/s. The eigen values are normalized by the sum of eigen values.

If the eigenvalues λ_i in figure 9 represent the amount of energy held by one mode, the two first modes capture 90% of the total energy fluctuations. POD allows us to reconstruct the evolution of gray level with the mean value and these two first modes of fluctuations:

$$\tilde{\mathbf{N}}_g = \bar{\mathbf{N}} + \sum_{k=1}^{2} a_k(t)\phi_k \tag{8}$$

The coherent structures with the smallest lengths are not taken into account in this reconstruction and it is a bit easier to analyse heat transfer. Some images representing the flow during one oscillation of the test with a welding speed of $2.3mm/s$ are shown in figure 10 after using equation 8 and temporal coefficients in figures 6 and 8.

If little deflection of the free surface is assumed, Marangoni effect is the dominant driving force near the free surface. The

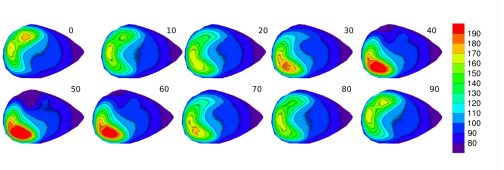

FIG. 10. Sequences of reconstruction of gray level according to equation 8.

shear stress created due to temperature difference leads to motion of fluid from hot to cold regions. The first image (image 0) is the initial state, with a higher temperature located at the top of the image. The surface tension gradient induced by temperature difference caused an inward flow (images 10 and 20 in figure 10). There is probably also a backward flow in the rear of the weld pool that can not be seen. Also, there is a heat input (images 30, 40 and 50) that can be seen on the surface with an increase in the temperature and size of the hot region. This heat input could be due to high temperature fluid flow coming from the top side at the contact point of the electric arc. There also appears to be a surface tension gradient that leads to an inverse inward flow to the left (top of the image) of the molten pool (images 70, 80 and 90).

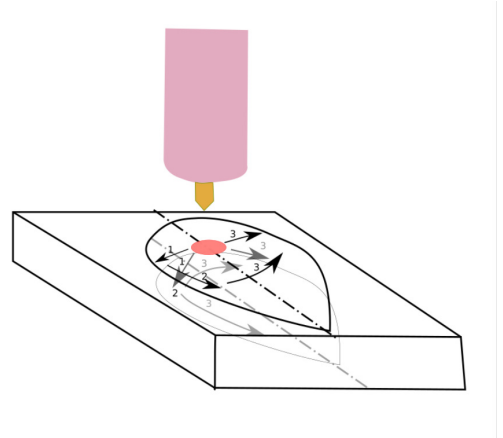

FIG. 11. Deduced fluid flow during one oscillation with POD mode reconstruction.

Figure 11 shows our interpretation of the series of images of the bottom side of the weld pool in terms of three dimensional heat transfer during a period of oscillation. At the top surface, the electric current distribution leads to a hot spot in the center of the weld pool. It is clear that the surface on the side of the arc is hotter. So heat goes away from the top surface to the bottom surface.

First, a part of the hot fluid is going to the left of the weld

pool at the top surface (label 1) and another part goes to the same side at the bottom. This leads to a hot point (label 2) at the bottom surface (image 40 in figure 10), and a large region that is subjected to a negative surface tension gradient which causes a flow directed inward and backward (label 3 on the bottom surface). A camera on the top surface observed also this motion which is synchronized with the camera capturing the bottom surface of the weld pool. The flow is now directed from the left side to the right side of the pool and the hot temperature is advected with fluid motion. This leads again to a hot spot at the end (label 3 or image 90 in figure 10). An alternative explanation is that this flow behavior is due to a strong interaction between the two symmetrical vortices in the middle of the weld pool and the front fusion boundary. If this boundary becomes asymmetric, the streams become also asymmetric and the vortices are not anymore symmetrical. To balance this phenomenon, the heat has to go from the hot vortex to the cold one leading again to an asymmetry of fusion boundary. Oscillations around a centerline between two vortices was recently observed in a simulation by Ebrahimi[21] in the same material and with a similar configuration.

The analysis presented here is based on a the gray level reconstruction. In reality, the situation is slightly more complex because small vortex structures exist alongside this main behaviour. However, this work demonstrates the interest in using POD to investigate fluid motion in the weld pool.

VI. CONCLUSION

In this paper, POD technique is used to investigate thermal field during GTAW. POD is based on the analysis of gray level of the weld pool captured by camera. The main advantages of this technique are that, once the exposure time and the aperture are set correctly, it is very simple and can be performed quickly. The technique is very powerful when fluctuations (turbulence or instabilities) exist in the fluid flow. It allows the temperature distributions to be decomposed into coherent structures and can be used to better understand the effect of the heat input. The material used here has a large Peclet number and so temperature distribution provides information on fluid flow pattern. In the present case, the decomposition into spatial modes allows us to explain the oscillations observed during two of the presented experimental tests. The technique is robust if there is no reflection for extraneous lights on the free surface which can complicate the analysis and is frequently encountered in industrial setting.

We must note at this point that the POD results are mainly qualitative as they are based on gray levels that are related to the surface temperature. Further developments will be to apply the POD with real surface temperature[22] in order to determine more precisely fluid velocities. Application of POD on the side of the arc can also reveal interesting results for the stability of heat transfer. Due to short running time, it is possible to implement this method whilst controlling the energy during the process in real time. Our analysis reveals oscillations modes that seems to suggest instabilities inside the weld pool. Further studies will be carried out in order to investigate the onset of the instabilities with respect to process parameters.

REFERENCES

[1] Tanaka.M, Terasaki.H, Ushio.M, and Lowke.J, "A Unified Numerical Modeling of Stationary Tungsten-Inert-Gas Welding Process", Metallurgical and Materials Transactions A, Vol 35, p2043-2052 ,2002

[2] Traidia.A and Roger.F, "Numerical and experimental study of arc and weld pool behaviour for pulsed current GTA welding", International Journal of Heat and Mass Transfer, Vol 54, p 2163-2179, 2011

[3] Chakraborty.N and Chakraborty.S and Dutta.P, "Modelling of turbulent transport in arc welding pools", International journal of numerical methods for heat and fluid flows, vol13, p7-30, 2003

[4] Kidess.A and Kenjeres.S and Kleijn.C, "The influence of surfactants on thermocapillary flow instabilities in low Prandtl metling pools", Physics of Fluids, Vol 28 , 2016, https://doi.org/10.1063/1.4953797

[5] Kraus.H.G, "Experimental Measurement of Thin Plate 304 Stainless Steel GTA Weld Pool Surface Temperatures", Welding Journal, p353-359, 1987

[6] Zacharia.T and David.S and Vitek.J and Kraus.H "Surface Temperature Distribution of GTA Weld Pools on Thin-Plate 304 Stainless Steel", Welding Journal, p 353-362, 1995

[7] Henrikson.P. "Visualisation of Weld Pool Surface Flow During TIG Welding of Stainless Steel 316L Plates" in Mathematical Modelling of Weld Phenomena 7, p125-147 , 2005

[8] Zhao.C.X and van Steijn.V and Richardson.I and Kleijn.C.R and Kenjeres.S and Saldi.Z, "Unsteady interfacial phenomena for weld poolinward flow with active surface oxide", Science and Technology of Welding and Joining, p , 2008

[9] Zhao.C.X, "Measurements of fluid flow in weld pools", Phd Thesis, TU Delft, 2011

[10] Aucott.L and Dong.H and Mirihanage.W and Atwood.R and Kidess.K and Gao.S and Wen.S and Marsden.J and Feng.S and Tong.M and Connolley.T and Drakopoulos.M and Kleijn.C and Richardson.I and Browne.D Mathiesen.R and Atkinson.H , "Revealing internal flow behaviour in arc welding and additive manufacturing of metals", Nature Communications, Vol9, 2018

[11] Aubry.N and Holmes.P and Lumley.J and Stone.E, "The dynamics of coherent structures in the wall region of a turbulent boundary layer", Journal of Fluid Mechanics, Vol 192, p 115-173, 1988

[12] Towne.A and Schmidt.O.T and Colonius.T, "Spectral proper orthogonal decomposition and its relationship to dynamic mode decomposition and resolvent analysis", Journal of Fluid Mechanics, Vol. 847, 821-867, 2018, doi:10.1017/jfm.2018.283

[13] Broumand.M and Asgarian.A and Bussmann.M and Chattopadhyay.K and Thomson.M, "Spatio-temporal dynamics and disintegration of a fan liquid sheet" , Physics of Fluids, Vol. 33, Issue 11, 2021 https://doi.org/10.1063/5.0063049

[14] Blanc.N and Soulié.F and Deschaux-Beaume.F and Bordreuil.C, *Submitted* , Science and Technology of Welding and Joining.

[15] Mills.K.C, Fe-316 Stainless Steel in "Recommended values of thermophysical properties for selected commercial alloys", Elsevier, p135-142

[16] Keene.B.J., Mills.K.C., Bryant.J.W. ,Hondros.E.D. , "Effects of interaction between surface active elements on the surface tension of iron", Canadian Metallurgy Quarterly p 393-403, 1982

[17] Bradski.G, "The OpenCV Library", Dr. Dobb's Journal of Software Tools, 2000

[18] Berkooz.G and Holmes.P and Lumley.J.L "The proper orthogonal decomposition in the analysis of turbulent flows" Annual Review Fluid Mechanics, Vol 25, p539–575, 1993

[19] Sirovich.L, "Turbulence and the dynamics of coherent structures. I - Coherent structures. ", Quarterly of Applied Mathematics, Vol 45,1987

[20] Rivas.B and Osrach, "Scaling of low-Prandtl-number thermocapillary flows", International Journal of Heat and Mass Transfer, Vol 35, p 1469-1479, 1992

[21] Ebrahimi.A and Kleijn.C and Hermans.M and Richardson.I, "The effects of process parameters on melt pool oscillatory behaviour in gas

tungsten arc welding", Journal of Physics: D Applied Physics, 16p https://doi.org/10.1088/1361-6463/abca62,2021

[22]Monier.R and Thumerel.F and Chapuis.J and Soulié.F and Bordreuil.c, "Liquid metals surface temperature fields measurements with a two-colour pyrometer", Measurement, Vol101, p72-80, 2017